THE JOURNAL OF PHYSICAL CHEMISTRY A
A JOURNAL OF THE AMERICAN CHEMICAL SOCIETY

pubs.acs.org/JPCA

Article

Enabling Molecular-Level Computational Description of Redox and Proton-Coupled Electron Transfer Reactions of Samarium Diiodide

Jonas Himmelstrup and Vidar R. Jensen*

Cite This: J. Phys. Chem. A 2023, 127, 3796−3803

Read Online

ACCESS | Metrics & More | Article Recommendations | Supporting Information

ABSTRACT: Samarium diiodide (SmI_2, Kagan's reagent) is a one-electron reductant with applications ranging from organic synthesis to nitrogen fixation. Highly inaccurate relative energies of redox and proton-coupled electron transfer (PCET) reactions of Kagan's reagent are predicted by pure and hybrid density functional approximations (DFAs) when only scalar relativistic effects are accounted for. Calculations including spin−orbit coupling (SOC) show that the SOC-induced differential stabilization of the Sm(III) versus the Sm(II) ground state is little affected by ligands and solvent, and a standard SOC correction derived from atomic energy levels is thus included in the reported relative energies. With this correction, selected meta-GGA and hybrid meta-GGA functionals predict Sm(III)/Sm(II) reduction free energies to within 5 kcal/mol of the experiment. Considerable discrepancies remain, however, in particular for the PCET-relevant O−H bond dissociation free energies, for which no regular DFA is within 10 kcal/mol of the experiment or CCSD(T). The main cause behind these discrepancies is the delocalization error, which leads to excess ligand-to-metal electron donation and destabilizes Sm(III) versus Sm(II). Fortunately, static correlation is unimportant for the present systems, and the error may be reduced by including information from virtual orbitals via perturbation theory. Contemporary, parametrized double-hybrid methods offer promise as companions to experimental campaigns in the further development of the chemistry of Kagan's reagent.

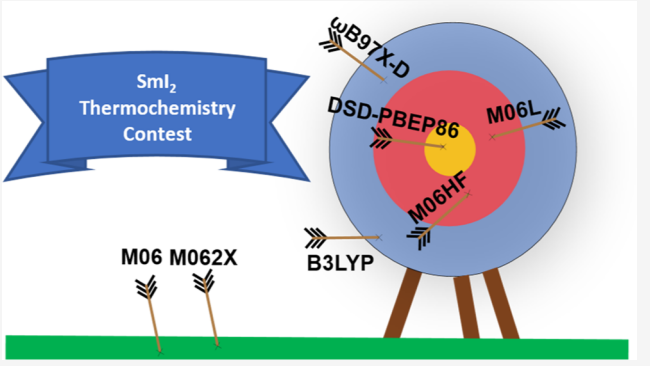

INTRODUCTION

Samarium diiodide, also known as Kagan's reagent, is an important reductant and, when combined with a Brønsted acid, a proton-coupled electron transfer (PCET) agent in a multitude of organic reactions.[1,2] Its PCET properties have also led to a recent breakthrough in low-temperature, homogeneously catalyzed ammonia synthesis, in which water, for the first time, acts as a proton source and stunning nitrogenase-like catalytic activities are obtained.[3] The widespread and varied use of Kagan's reagent in organic chemistry and its new role in the development of alternative ammonia production processes should be complemented by molecular-level computational studies to provide insights and to spur further progress.

Illustrating the drive to obtain fundamental insights via synergistic use of calculations and experiments are a series of recent studies of the solution-based coordination chemistry of SmI_2[2,4−6] and of C−C bond formation reactions initiated by a single-electron transfer (SET) from Sm(II) to redox-active ligands.[7] However, only a couple of computational studies have so far targeted the energetics associated with the one-electron oxidation of SmI_2.[4,8] The reason for this lack of computational studies of the very process that is key to the reactivity of SmI_2 is presumably rooted in the challenges involved in describing this one-electron oxidation using standard density functional approximations (DFA). These challenges have been thoroughly demonstrated by Maron and Perrin and co-workers,[9] who concluded that it is "more imperative than ever" to identify "a general method or strategy that will be simple and effective" in describing the redox chemistry and SET processes of SmI_2.

Here, we answer this call by analyzing two exemplary processes key to the reactivity of SmI_2: the one-electron reduction of $SmI_2(THF)_5^+$ and the PCET-relevant bond dissociation free energy (BDFE) of an O−H bond of $SmI_2(THF)_4H_2O$, both in tetrahydrofuran (THF) solution. The performance of density functionals of up to the fifth rung of Jacob's ladder[10] is compared to experimental estimates. To further validate the PCET-relevant performance, BDFEs for a smaller model complex, $SmI_2(H_2O)_5$, are compared to those of the coupled cluster method CCSD(T). Finally, the results are rationalized in terms of electron correlation, exchange, and the

Received: January 18, 2023
Revised: March 24, 2023
Published: April 19, 2023

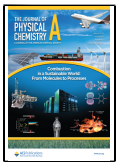

delocalization error (DE) of DFAs. The associated insights and recommendations will be useful for future computational contributions to the understanding and development of the rich chemistry driven by electrons from SmI_2.

COMPUTATIONAL METHODS

All density functional theory (DFT) calculations were performed using the C.01 version of the Gaussian16 package.[11] For spin multiplicities >1, unrestricted calculations were performed. Significant spin contamination was not observed.

Geometry Optimizations. The hybrid meta exchange−correlation functional PW6B95[12] complemented by Grimme-type D3 empirical dispersion[13] with Becke−Johnson damping,[14,15] here labeled PW6B95-D3(BJ), was used for geometry optimizations. The PW6B95-D3(BJ)-optimized geometry of $SmI_2(THF)_5^+$ compares excellently with the corresponding single-crystal X-ray structure, with the optimized Sm−O and Sm−I distances only being slightly (ca. 1%) longer than those of the X-ray structure (see Section S2.1 in the Supporting Information). A similar pattern of slight overestimation of Sm−ligand distances is seen when comparing the optimized Sm−O and Sm−I distances of $SmI_2(THF)_4H_2O$ with those obtained from in situ X-ray absorption spectroscopy on a 1:1 mixture of SmI_2 and water in THF.[16] More generally, the PW6B95 functional, with or without empirical dispersion corrections, has been found to perform well across a broad range of transition-metal chemistry,[17] including the prediction of spin-state stability,[18] as well as main-group chemistry.[19,20]

The input geometries of $SmI_2(THF)_5/SmI_2(THF)_5^+$ were taken from ref 8, in which the structure of SmI_2 in THF has been explored computationally. In the latter work, SmI_2 was found to coordinate five THF molecules, forming the coordinatively saturated $SmI_2(THF)_5$, with the two iodide ligands located trans to each other. This is consistent with the single-crystal structure determined for SmI_2 crystallized from THF.[21] For $SmI_2(THF)_4H_2O$ and $SmI_2(THF)_4OH$, input geometries were generated by replacing, using a molecular builder, a THF moiety by water and hydroxide, respectively. Similar procedures were followed when generating input geometries for $SmI_2(H_2O)_5$ and $SmI_2(H_2O)_4OH$.

Solvent effects were included in the geometry optimizations by using the SMD continuum solvation model for THF.[22] The cavity was constructed by adding the solvent radius to the unscaled atomic radii (surface = SAS). The self-consistent field (SCF) convergence criterion was tightened 10-fold (SCF (conver = 9)) compared to the default, and the wavefunction was tested for instabilities (stable = opt) at the start of the geometry optimization. Geometries were optimized to a maximum force of 1.5×10^{-5} au (opt = tight). For SCF energies and gradients, numerical integrations were performed using Gaussian's "ultrafine" grid (a pruned 99,590 grid with 99 radial shells and 590 angular points per shell), whereas Gaussian's "finegrid" (a pruned 75,302 grid with 75 radial shells and 302 angular points per shell) was used for the CPHF analytical Hessian calculations. The eigenvalues of the analytically calculated Hessian were used to characterize stationary points, confirming positive curvatures (or no imaginary frequencies) for the minima.

The basis sets for geometry optimization were as follows: for H and C, correlation-consistent valence double-ζ plus polarization (cc-pVDZ) basis sets were used.[23] For O, a correlation-consistent valence double-ζ plus polarization basis set augmented by diffuse s, p, and d functions (aug-cc-pVDZ) was used.[23−27] For I, a relativistic 28-electron Stuttgart/Cologne effective core potential (ECP28MDF) was used in conjunction with an accompanying correlation-consistent valence double-ζ plus polarization basis set augmented by diffuse s, p, and d functions (aug-cc-pVDZ-PP).[28,29] For Sm in oxidation state +II, a quasi-relativistic 52-electron Stuttgart/Cologne ECP (ECP52MWB) was combined with an accompanying (7s6p5d) primitive basis set contracted to [5s4p3d].[30,31] With the ECP incorporating the unpaired electrons, singlet spin multiplicity was used when geometry optimizing spin-septet Sm(II) complexes. Similarly, for Sm in oxidation state +III, a quasi-relativistic 51-electron Stuttgart/Cologne ECP (ECP51MWB) was combined with an accompanying (7s6p5d)/[5s4p3d] basis set. With the ECP incorporating the unpaired electrons, singlet spin multiplicity was used when geometry optimizing spin-sextet Sm(III) complexes.

The ECPs and basis sets of the geometry optimizations were taken from the basis set exchange server,[32−34] except for Sm, for which the Stuttgart/Cologne website was used.[35] See Table S1 for an overview of the basis sets used for geometry optimization.

Single-Point Calculations. Single-point (SP) calculations at the optimized geometries were performed using more flexible basis sets and a range of different computational methods (see Table S2 for an overview). The SCF density-based convergence criterion was set to rms $<1.0 \times 10^{-5}$ and maximum change $<1.0 \times 10^{-3}$ (keyword SCF (conver = 5)) for the DFT calculations. For the double-hybrid and coupled-cluster calculations, the SCF convergence criterion was set to "tight", and the chemical valence electrons of O, C, and H atoms were included in the correlation treatment, whereas the core electrons were frozen. For I, the 4d electrons were included in the correlation treatment in addition to the 5s and 5p valence electrons. For Sm, the 4d, 5s, 5p, 4f, and 6s electrons were included in the correlation treatment.

Unless otherwise stated, solvent effects of THF were included in the SP calculations via the SMD continuum solvation model,[22] with the cavity built using scaled atomic radii. Natural atomic charges and electron populations were obtained from natural bond orbital (NBO) analyses using the NBO7 software.[36] In the double-hybrid calculations, the option "density = current" was included to ensure that the NBO analyses were performed on the final double-hybrid density.

The basis sets used in the SP calculations were as follows: for H and C, correlation-consistent valence triple-ζ plus polarization (cc-pVTZ) basis sets were used.[23] For O, a correlation-consistent valence triple-ζ plus polarization basis set augmented by diffused s, p, and d functions (aug-cc-pVTZ) was used.[23−27] For I, a relativistic Stuttgart/Cologne 28-electron ECP (ECP28MDF) was used in conjunction with an accompanying valence triple-ζ plus polarization basis set augmented by diffuse s, p, and d functions (aug-cc-pVTZ-PP).[28,29]

For Sm, a quasi-relativistic 28-electron Stuttgart/Cologne ECP (ECP28MWB) was used in conjunction with an accompanying segmented (14s13p10d8f6g)/[10s8p5d4f3g] basis set.[37,38] With no unpaired electrons included in the ECP, septet and sextet spin multiplicities were used in the SP calculations on Sm(II) and Sm(III) complexes, respectively.

https://doi.org/10.1021/acs.jpca.3c00418
J. Phys. Chem. A 2023, 127, 3796−3803

The ECPs and basis sets of the SP calculations were taken from the basis set exchange server,[32−34] except for Sm, for which the Stuttgart/Cologne website was used.[35] See Table S3 for an overview of the basis sets used in the SP calculations.

Basis set superposition errors (BSSE) affecting the BDFE of $SmI_2(THF)_4H_2O$ (fragments: $SmI_2(THF)_4OH$ and H) and $SmI_2(H_2O)_5$ (fragments: $SmI_2(H_2O)_4OH$ and H) were calculated using the counterpoise method in conjunction with the above SP basis sets for DFT. The functionals selected for BSSE calculation were M06L-D3, PW6B95-D3(BJ), and DSD-PBEP86, thus spanning rungs 3−5. The BSSE was found to be small in all cases (0.1−0.3 kcal/mol for the regular DFAs and 0.7 kcal/mol for the double-hybrid method; see Tables S7 and S8), and the reported BDFEs are thus not corrected for BSSE.

Estimates of spin−orbit coupling (SOC) effects were obtained via SP calculations using the 5.03 version of the ORCA package.[39] Using the second-order Douglas−Kroll−Hess (DKH) Hamiltonian[40,41] and the SMD solvation model throughout,[22] all-electron, complete active space SCF (CASSCF) calculations with an active space consisting of seven orbitals and six and five electrons, respectively, for Sm(II) (CASSCF(6,7)) and Sm(III) (CASSCF(5,7)) were used to generate zeroth-order wavefunctions for the subsequent strongly contracted N-electron valence perturbation theory (SC-NEVPT2) treatment,[42−44] in which the correlation treatment involved the same electrons as described above for the coupled-cluster calculations. The CASSCF wavefunctions were averaged over the seven (^{7}F) and 21 (^{6}H°) roots of the spin-septet and sextet atomic Sm^{2+} and Sm^{3+} terms, respectively. The converged active orbitals were quite pure Sm 4f orbitals. SOC effects were estimated via quasi-degenerate perturbation theory (QDPT)[45,46] using an approximate Breit−Pauli mean-field SOC operator, termed RI-SOMF(1X),[47] in which the exchange term is obtained via one-center exact integrals including the spin-other orbit interaction, and the Coulomb term is computed using the resolution of the identity approximation. The QDPT treatment used a basis of roots of the Born−Oppenheimer Hamiltonian, with the matrix elements computed over the state-averaged CASSCF wavefunctions, but with NEVPT2 energies along the diagonal of the QDPT matrix, accounting for dynamic correlation effects.

The orbital basis sets used in the all-electron SOC calculations were built-in ORCA basis sets, as detailed in the following: O, C, and H atoms were described by DKH-def2-TZVP basis sets, which are def2-TZVP basis sets[48] recontracted for DKH by D. A. Pantazis. I atoms were described by segmented all-electron relativistically contracted (SARC) basis sets of the SARC-DKH-TZVP type.[49] Sm atoms were described by the SARC2-DKH-QZVP basis set.[50] Accompanying auxiliary SARC/J basis sets were used for Coulomb fitting, implying decontracted def2/J sets for O, C, and H atoms,[51] and SARC/J sets for I,[49] and Sm.[52]

Calculation of Gibbs Free Energies. Thermochemical corrections ($G^{THF\ 298K}_{PW6B95\text{-}D3(BJ)\ qh}$) to give Gibbs free energies were calculated at the geometry optimization level at 298 K using the ideal gas, rigid rotor, and harmonic oscillator approximations, except that frequencies below 100 cm^{-1} were shifted to 100 cm^{-1} when calculating the vibrational entropy (i.e., the quasi-harmonic oscillator approximation, here indicated using a subscript "qh")[53] to correct for the breakdown of the harmonic oscillator model for entropies of low-frequency vibrational modes. The Gibbs free energy of a system was thus obtained using eq 1.

$$G^{THF\ 298K} = E^{THF} + G^{THF\ 298K}_{PW6B95\text{-}D3(BJ)\ qh} + G^{298K}_{1atm\rightarrow 1M} \quad (1)$$

$G^{298K}_{1atm\rightarrow 1M}$ is the standard state correction corresponding to a 1 M solution, amounting to 1.89 kcal/mol (=RT ln(24.46)) at room temperature. E^{THF} is the potential energy resulting from an SP calculation using the above-described (quasi-)relativistic ECPs. Including the SOC-induced differential stabilization, $\Delta E^{SOC} = E^{SOC}(Sm(III)) - E^{SOC}(Sm(II))$, of the Sm(III) versus the Sm(II) ground state, the reaction free energy in THF was calculated using eq 2.

$$\Delta G = G^{THF\ 298K}_{products} - G^{THF\ 298K}_{reactants} + \Delta E^{SOC} \quad (2)$$

The corresponding reaction free energy in the gas phase (limited to the BDFE for $SmI_2(H_2O)_5$ reported in Table S6) was calculated using eq 3.

$$G^{GAS\ 298K} = E^{GAS} + G^{THF\ 298K}_{PW6B95\text{-}D3(BJ)\ qh} \quad (3)$$

E^{GAS} is the potential energy resulting from an SP calculation with a given method without applying the SMD solvation model. The reaction free energy (ΔG) was subsequently calculated using eq 4.

$$\Delta G = G^{GAS\ 298K}_{products} - G^{GAS\ 298K}_{reactants} + \Delta E^{SOC} \quad (4)$$

RESULTS AND DISCUSSION

SOC Effects. SOC is a relativistic phenomenon which increases in importance with the nuclear charge. Since our computational models for estimation of the energy (E^{THF}) of Sm(II) and Sm(III) complexes in THF solution only include scalar relativistic effects via quasi-relativistic ECPs, we here estimate the stabilization, expressed as a negative E^{SOC}, of the ground states of these complexes induced by SOC.

As seen in Table 1, the SOC effect on the ground-state energy of Sm^{2+} and Sm^{3+} ions is mildly underestimated in the calculations compared to those taken as the difference between the $^7F_0$ and $^6H^o_{5/2}$ ground states, respectively, and the average levels of the corresponding ^{7}F and ^{6}H° terms of the atomic spectra.[54] More importantly, the differential stabilization of

Table 1. SOC-Induced Stabilization of Sm(II) and Sm(III) Ground States

system	calc/expt.	E^{SOC} [cm^{-1}]	ΔE^{SOC} [kcal/mol]
Sm^{2+} free ion	expt.[a]	−2503.99	
Sm^{3+} ion in $LaCl_3$	expt.[a]	−3761.21	−3.59
Sm^{2+} free ion	calc.	−2234.97	
Sm^{3+} free ion	calc.	−3680.29	−4.13
Sm^{2+} ion in THF	calc.[b]	−2232.27	
Sm^{3+} ion in THF	calc.[b]	−3682.18	−4.15
$SmI_2(H_2O)_5$ in THF	calc.[b]	−2050.50	
$SmI_2(H_2O)_5^+$ in THF	calc.[b]	−3547.44	−4.28
$SmI_2(H_2O)_4OH$ in THF	calc.[b]	−3550.52	−4.29

[a]From the spectrum of the free Sm^{2+} ion or from that of Sm^{3+} in $LaCl_3$.[54] [b]From calculations including continuum solvation effects of THF via the SMD model.

https://doi.org/10.1021/acs.jpca.3c00418
J. Phys. Chem. A 2023, 127, 3796−3803

Table 2. Calculated Energetics and Natural Electron Populations (N) and Charges (q) of the Reduction of $SmI_2(THF)_5^+$ to $SmI_2(THF)_5$ in THF[a]

				$SmI_2(THF)_5^+$			$SmI_2(THF)_5$		
entry	method[b]	% HF exchange	ΔG^c [kcal/mol]	N (4f)	N (5d)	q (Sm)	N (4f)	N (5d)	q (Sm)
1	HF	100	−48.3	5.01	0.74	2.01	6.00	0.34	1.53
2	LSDA	0	−92.3	5.41	0.96	1.36	5.98	0.52	1.31
3	PBE[d]	0	−92.3	5.37	0.93	1.44	5.98	0.48	1.36
4	PBE-D3(BJ)[d]	0	−87.5	5.37	0.93	1.44	5.98	0.48	1.36
5	M06L-D3	0	−83.0	5.30	0.92	1.52	5.98	0.47	1.39
6	TPSS-D3(BJ)[e]	0	−82.6	5.32	0.93	1.50	5.98	0.47	1.38
7	PW6B95-D3(BJ)	28	−89.9	5.09	0.95	1.70	5.99	0.43	1.41
8	B3LYP-D3(BJ)	20	−86.7	5.13	0.93	1.68	5.99	0.43	1.42
9	M06-D3	27	−104.3	5.24	0.91	1.59	5.99	0.46	1.39
10	M062X-D3	54	−99.8	5.04	0.90	1.78	6.00	0.43	1.41
11	M06HF-D3	100	−82.3	5.04	0.83	1.89	6.00	0.40	1.45
12	PBEQIDH-D3(BJ)	69.3	−78.1	5.02[f]	0.94[f]	1.75[f]	5.97	0.43	1.42
13	DSD-PBEP86	69	−78.2	5.00	0.70	2.06	5.97	0.45	1.40
14	revDSD-PBEP86	69	−75.7	5.01	0.70	2.06	5.98	0.45	1.41
15	B2PLYP-D3(BJ)	53	−78.6	5.03	0.97	1.71	5.97	0.45	1.40
16	expt.[g]		−80.7						

[a]Energies and properties obtained in SP calculations using the SMD continuum solvation model for the THF solvent on geometries optimized using the PW6B95-D3(BJ) functional. Population analysis was carried out according to the NPA/NBO scheme. [b]See the Supporting Information for the definition of the methods. [c]Calculated using eq 2. [d]Combination of the PBE exchange functional and the PBE correlation. [e]Combination of the TPSS exchange functional and the TPSS correlation. [f]Calculated using the "FixDM" keyword. [g]Calculated from ref 57 using eqs 5 and 6.

Sm^{3+} versus Sm^{2+} is well reproduced, with $|\Delta E^{SOC}|$ being overestimated by only ca. 0.5 kcal/mol. Also important, whereas the inclusion of solvent effects and ligands reduces the SOC-induced stabilization of the Sm(II) and Sm(III) ground states, ΔE^{SOC} appears to be little affected by the environment of the Sm^{n+} ions. Only minor increases in $|\Delta E^{SOC}|$ are obtained on the inclusion of continuum solvation effects (for THF) and coordinating iodide, water, and hydroxide ligands in the calculations. Limited environmental influence on the SOC-induced stabilization is also indicated by the levels of the Sm^{3+} $^6H^o$ term observed in various solvents[55,56] being comparable to those of Sm^{3+} ions in $LaCl_3$.[54]

In conclusion, due to the limited influence of the environment on the SOC ground-state stabilization, we adopt the stabilization derived from the atomic spectra of Sm^{2+} and Sm^{3+} ions. In other words, $\Delta E^{SOC} = -3.59$ kcal/mol (product: Sm(III)) or $\Delta E^{SOC} = 3.59$ kcal/mol (product: Sm(II)) has been used in eqs 2 and 4 to correct relative free energies calculated using quasi-relativistic ECPs (parameterized to account for scalar relativistic effects) for SOC-induced differential stabilization of Sm(III) versus Sm(II).

Reduction of SmI_2^+. First, the most straightforward test that any method applied to the study of reactions involving SmI_2 as a reductant can be subjected to is to predict the corresponding one-electron reduction potential. The experimental reduction potential of SmI_2^+ has been reported to be −1.41 V versus Fc^+/Fc (Fc = ferrocene) in THF at room temperature,[57] which is equivalent to −0.78 V versus NHE (NHE = normal hydrogen electrode).[58,59] Thus, the absolute reduction potential (E^0_{abs}) in THF is given by eq 5.[60,61]

$$E^0_{abs} = E^0_{NHE} + 4.281\ \text{V} \quad (5)$$

Consequently, $E^0_{abs} = 3.50$ V for SmI_2^+, and the corresponding ΔG^0_{red} of the reduction can be obtained from eq 6.

$$\Delta G^0_{red} = -nFE^0_{abs} \quad (6)$$

where n is the number of electrons transferred, and F is the Faraday constant. Thus, the experimentally determined one-electron reduction potential of SmI_2^+ corresponds to a reaction free energy of −80.7 kcal/mol, which is the estimate against which reduction free energies calculated for $SmI_2(THF)_5^+/SmI_2(THF)_5$ are compared (Table 2; additional results, including reduction potentials, in Table S4).

As expected for an electron uptake, the estimated reaction energy is very sensitive to the correlation treatment. Whereas Hartree−Fock, lacking electron correlation, underestimates the stability of the reduced neutral complex by almost 33 kcal/mol (entry 1, Table 2), the DFAs overestimate the exergonicity, or equivalently, the reduction potential, to varying degrees. Still, compared to HF, even standard first- and second-rung functionals (entry 2−4) roughly halve the errors. Accounting for dispersion stabilizes the more compact $SmI_2(THF)_5^+$ complex (the average Sm−O(THF) distance is 0.15 Å shorter than in $SmI_2(THF)_5$; see Figure S1 for optimized geometries) and cuts the overestimation of the exergonicity to ca. 7 kcal/mol (entry 4). Including dependency on the kinetic energy density in the exchange−correlation functional (third rung) reduces the error by another 4−5 kcal/mol (entry 5−6).

In contrast, including moderate components of exact (HF) exchange, as in popular, dispersion-including, fourth-rung functionals such as B3LYP-D3(BJ), M06-D3, and M062X-D3 (entry 8−10), and various range-separated functionals (Table S4), invariably leads to larger errors. A significant improvement over the third rung is only seen when large components of exact (HF) exchange are included. The effect of HF exchange is particularly striking for the hybrid Minnesota functionals (entry 9−11). M06-D3 and M062X-D3 overestimate the stability of the neutral complex relative to the cationic complex by almost 23.6 and 19.1 kcal/mol, respectively. Only on the inclusion of 100% HF exchange is this overestimation reduced to below 2 kcal/mol (M06HF-D3, entry 11). The improvements resulting from terms involving kinetic-energy density and from large components of HF exchange are diagnostic of

https://doi.org/10.1021/acs.jpca.3c00418
J. Phys. Chem. A 2023, 127, 3796−3803

the DE (which includes the self-interaction error) of DFAs.[62] The DE may all but disappear when combining HF exchange with second-order perturbative correlation treatment.[62] Indeed, whereas the regular, DE-suffering DFAs all overestimate the exergonicity of the reduction, the double-hybrid methods undershoot, but not by much. Except for revDSD-PBEP86[63] (off by 5 kcal/mol), they are within 3 kcal/mol of the experiment (entry 12−15).

The magnitude of the DE for lanthanide complexes has been found in detailed work by Duignan and Autschbach[64] to correlate with the lanthanide 4f and 5d electron populations. The likely explanation for this correlation is that the DE leads to artificial mixing of metal and ligand orbitals, excess ligand-to-metal electron donation (i.e., delocalization), and exaggerated 4f and 5d populations.[64] Indeed, here the DE-free HF and presumably DE-free double-hybrid methods predict the combined 4f and 5d populations of $SmI_2(THF)_5^+$ to be 0.30−0.60 lower than those of standard GGA-based DFAs (cf., entry 4 and 12−15, Table 2), resulting in a more positively charged Sm center.

O−H BDFE of $SmI_2(THF)_4H_2O$. Having identified methods predicting the energetics of the $SmI_2(THF)_5^+/SmI_2(THF)_5$ reduction with excellent accuracy and little interference from the DE, we next turned to a PCET-relevant reaction for which the energetics can be expected to depend on the Sm(II)/Sm(III) relative stability: the rupture of a O−H bond of $SmI_2(THF)_4H_2O$ to give $SmI_2(THF)_4OH$ and $H^\bullet$. The BDFE of PCET reactions can be estimated from experimental parameters using eq 7.[65]

$$\mathrm{BDFE} = 1.364\ \mathrm{p}K_a + 23.06E^0 + C_G \quad (7)$$

Here, to estimate the BDFE resulting from mixing 1 equiv of water with SmI_2 in THF solution, we note that the most relevant pK_a available is that of $SmI_2{-}H_2O$ in water, reported to be 7.11.[66] Similarly, the most applicable reduction potential E^0 is that for SmI_2 in THF, which is −1.41 V versus Fc^+/Fc.[57] We assume negligible changes in E^0 on the replacement of a THF by a water molecule. Next, C_G is the free energy of H^+/H_2 reduction, reported to be 60.4 kcal/mol in THF.[66] Thus, the BDFE of the PCET conducted by $SmI_2(THF)_4H_2O$ in THF can be estimated to 37.6 kcal/mol. Lower estimates have been made for more water-rich mixtures,[67] but excess water increases the reductive power[2,68] and thereby lowers the BDFE, of SmI_2. For the present 1:1 water/SmI_2 mixture, eq 7 in conjunction with the above experimental information is assumed to offer the best estimate of our PCET-relevant BDFE (37.6 kcal/mol). This is thus the estimate against which a selection of BDFEs calculated using methods of rung 3−5 for $SmI_2(THF)_4H_2O$ are compared (Table 3; additional results in Table S5).

As for the above reduction free energies, the best-performing methods of Table 3 tend to stabilize Sm(III) versus Sm(II), thereby predicting lower BDFEs. However, as already indicated by the presence of components other than E^0 in eq 7, the BDFE is harder to predict. DFAs estimating the reduction free energy to within 2−3 kcal/mol, such as M06L-D3 and M06HF-D3, are, with errors of 12−13 kcal/mol, unsuitable for predicting the BDFE. To analyze the physical origins of these errors, we note that an O−H σ-bond and a dative $Sm{-}OH_2$ bond are replaced by a short, polar Sm−OH bond (2.15 Å, 9 pm shorter than the minimum Sm−O distance in a distribution of bond distances between Sm^{3+} and O^{2-} ions determined by X-ray crystallography).[69] The close Sm−O contact suggests that correlation effects of the Sm(III) state influence the BDFE more than the $SmI_2(THF)_5^+/SmI_2(THF)_5$ reduction potential. This is likely the reason why mixed performance is observed even among double-hybrid methods. Combined with empirical dispersion corrections (D3(BJ)), B2PLYP, one of the first double-hybrid methods to be suggested,[70] predicts a BDFE that is almost 8 kcal/mol too high, whereas subsequently developed double-hybrid methods (DSD-PBEP86,[71] and PBEQIDH-D3(BJ)),[72,73] consistent with their improved performance in validation studies,[74,75] are within 2 kcal/mol of the experimental estimate. As for the above one-electron reduction (Table 2), the reparametrized DSD-PBEP86 functional, revDSD-PBEP86,[63] overestimates the stability of the +III versus the +II oxidation state of Sm and predicts a BDFE that is too low by almost 4 kcal/mol (Table S5). Still, even with this spread among the double-hybrid methods, we note that they all predict the BDFE to within 8 kcal/mol of the experiment and that their average prediction (38.2 kcal/mol) is within 1 kcal/mol. In contrast, the best DFAs of rungs three and four all overshoot the BDFE by at least 10 kcal/mol, and many popular hybrid DFAs, such as the long-range-corrected ωB97X-D functional[76] (Table S5), are associated with errors on the order of 20 kcal/mol.

Table 3. O−H BDFEs of $SmI_2(THF)_4H_2O$ in THF[a]

entry	method[b]	BDFE[c] [kcal/mol]
1	M06L-D3	49.6
2	TPSS-D3(BJ)	53.4
3	PW6B95-D3(BJ)	59.8
4	M06HF-D3	51.0
5	PBEQIDH-D3(BJ)	36.2
6	DSD-PBEP86	37.3
7	B2PLYP-D3(BJ)	45.4
8	expt.[d]	37.6

[a]See Table S5 for additional calculated BDFEs. [b]See Table S2 for definitions of the methods. [c]Calculated using eq 2. [d]Obtained from experimental parameters using eq 7.

O−H BDFE of $SmI_2(H_2O)_5$. To test whether the above agreement between the BDFE predicted by the best double-hybrid methods and the experiment might be the result of a fortuitous cancellation of errors, for example, involving continuum-model solvent effects, corresponding BDFEs were also calculated for the model complex $SmI_2(H_2O)_5$, the geometry of which was optimized starting from the Sm and O positions of $SmI_2(THF)_4H_2O$ (Figure S1). For the small water-based model complex, BDFE could be obtained using the coupled-cluster CCSD(T) method,[77] which involves single and double substitutions of the HF reference along with a perturbative estimate of connected triples. Thus, the water-based model complex allowed for comparing gas-phase DFT-predicted BDFEs directly with those obtained using CCSD(T), thereby circumventing the impact of the solvent model in the validation. Other uncertainties are also cancelled out, such as those associated with the SOC-induced differential stabilization of the Sm^{n+} ground states: all the BDFEs calculated for $SmI_2(H_2O)_5$ have been corrected with the same standard correction (ΔE^{SOC} = −3.59 kcal/mol) to account for SOC stabilizing Sm(III) more than Sm(II).

Before proceeding to the gas-phase calculations, we note that the BDFE predicted for $SmI_2(H_2O)_5$ in THF is lower (by 6 kcal/mol, cf. entry 2 in Table 4 vs entry 3 in Table 3) than that for $SmI_2(THF)_4H_2O$, consistent with the observed

https://doi.org/10.1021/acs.jpca.3c00418
J. Phys. Chem. A 2023, 127, 3796−3803

Table 4. O−H BDFEs of $SmI_2(H_2O)_5$ in the Gas Phase[a]

entry	method[b]	BDFE[c] [kcal/mol]
1	M06L-D3	41.7
2	PW6B95-D3(BJ)[d]	53.8
3	PW6B95-D3(BJ)	48.7
4	M06HF-D3	44.9
5	PBEQIDH-D3(BJ)	35.7
6	DSD-PBEP86	28.8
7	CCSD	29.1
8	CCSD(T)	28.3

[a]See Table S6 for additional calculated BDFEs. [b]See Table S2 for definitions of the methods. [c]Calculated using eq 4. [d]Including THF solvent effects via the SMD continuum solvation model.

increased reducing power and lowering of the BDFE on addition of water to solutions of SmI_2.[2,68] Removing the continuum solvent treatment further lowers the BDFE by 3.3 kcal/mol (entry 3, Table 4). Consequently, the CCSD(T)-predicted BDFE for $SmI_2(H_2O)_5$ in the gas phase (28.3 kcal/mol, entry 8 in Table 4) is lower than the experimental estimate for $SmI_2(THF)_4H_2O$ in THF (37.6 kcal/mol, entry 8 in Table 3). With the T1 diagnostic being well below 0.02[78] for both $SmI_2(H_2O)_5$ (0.0113) and $SmI_2(H_2O)_4OH$ (0.0124), the CCSD(T)-predicted BDFE is here taken as the value against which the methods of Table 3 are compared. Moreover, the low T1 values indicate that neither Sm(II) nor Sm(III) is heavily influenced by nondynamical correlation and that most of the correlation effects may be recovered perturbatively.

This is confirmed by the double-hybrid methods, which, as for Table 3 above, are alone in predicting BDFEs within 10 kcal/mol of CCSD(T) and in being reasonably well centered around this reference. The methods with the smallest deviation from CCSD(T) are the two double hybrids that include spin-component scaling of the MP2-like correlation, DSD-PBEP86 and revDSD-PBEP86 (Table S6). The performance of the original DSD-PBEP86 functional is particularly impressive, with both BDFEs being within 1 kcal/mol of the reference (Tables 3 and 4) and the reduction free energy (Table 2) being within 3 kcal/mol. The spin-component scaling enables, via parametrization, more of the correlation effects to be captured, and the two DSD functionals are also the methods with the highest reported general accuracy among the double-hybrid methods used here.[74] It seems plausible that spin-component scaling better captures the correlation effects of the compact Sm(III) water complex, in which the Sm−O bond (2.11 Å) is even shorter than that of $SmI_2(THF)_4OH$ (2.15 Å). Finally, the highly accurate relative free energies predicted here by DSD-PBEP86, in particular, together with those of a challenging C−C bond forming reaction initiated by SET from SmI_2,[7] suggest that DSD-PBEP86 and other spin-component-scaled and parametrized double-hybrid methods might represent the "simple and effective" strategy called for[9] to describe the redox and SET chemistry of SmI_2.

CONCLUSIONS

The true density functionals, that is, DFAs depending only on the density or quantities derived directly from the density, tested here are unsuitable for predicting energetics of redox and PCET processes of SmI_2 when only accounting for scalar relativistic effects. Fortunately, the differential SOC-induced stabilization of the Sm(III) versus the Sm(II) ground state appears to be little influenced by ligands and solvent. Correcting the relative energies with a standard differential (ΔE^{SOC}) derived from atomic spectra improves the agreement with the experiment and brings a couple of common meta-GGAs (M06L-D3 and TPSS-D3(BJ)) and a hybrid meta-GGA functional with 100% exact exchange (M06HF-D3) to within 5 kcal/mol of the experimental reduction free energy of the Sm(III)/Sm(II) redox couple. Still, even with SOC corrections, the most accurate functionals overshoot O−H BDFEs of SmI_2-induced PCET reactions by more than 10 kcal/mol, with many popular GGAs and hybrid-GGA functionals predicting BDFEs that are 15−20 kcal/mol too high. Most of this failure of regular DFAs is caused by the DE, which leads to excess ligand-to-metal electron donation and destabilizes the +III versus the +II oxidation state of Sm. Fortunately, the present systems do not appear to be heavily influenced by non-dynamical correlation effects, and including information from virtual orbitals via perturbation theory, as in double-hybrid methods, reduces the DE and improves the predicted energetics significantly. In particular, the high accuracy obtained here for DSD-PBEP86 is promising with respect to the use of this and other spin-component scaled and parametrized double-hybrid methods in future studies of the rich redox-related chemistry of SmI_2.

ASSOCIATED CONTENT

Supporting Information

The Supporting Information is available free of charge at https://pubs.acs.org/doi/10.1021/acs.jpca.3c00418.

Additional computational details and results (PDF)

Cartesian coordinates of optimized complexes (XYZ)

AUTHOR INFORMATION

Corresponding Author

Vidar R. Jensen − *Department of Chemistry, University of Bergen, N-5007 Bergen, Norway;* orcid.org/0000-0003-2444-3220; Email: Vidar.Jensen@uib.no

Author

Jonas Himmelstrup − *Department of Chemistry, University of Bergen, N-5007 Bergen, Norway;* orcid.org/0000-0001-6168-5128

Complete contact information is available at: https://pubs.acs.org/10.1021/acs.jpca.3c00418

Notes

The authors declare no competing financial interest.

ACKNOWLEDGMENTS

The Research Council of Norway (RCN, via grants 333151, NN2506K, and NS2506K) is gratefully acknowledged for financial support and computing and storage resources. The University of Bergen is acknowledged for a PhD scholarship to J.H. A reviewer is thanked for encouraging an investigation of SOC effects, and a colleague (Knut J. Børve) is thanked for helpful discussions on how to best perform this investigation.

REFERENCES

(1) Szostak, M.; Fazakerley, N. J.; Parmar, D.; Procter, D. J. Cross-Coupling Reactions Using Samarium(II) Iodide. *Chem. Rev.* **2014**, *114*, 5959−6039.

(2) Ramírez-Solís, A.; Boekell, N. G.; León-Pimentel, C. I.; Saint-Martin, H.; Bartulovich, C. O.; Flowers, R. A. Ammonia Solvation vs

Aqueous Solvation of Samarium Diiodide. A Theoretical and Experimental Approach to Understanding Bond Activation Upon Coordination to Sm(II). *J. Org. Chem.* **2022**, *87*, 1689−1697.
(3) Ashida, Y.; Arashiba, K.; Nakajima, K.; Nishibayashi, Y. Molybdenum-Catalysed Ammonia Production with Samarium Diiodide and Alcohols or Water. *Nature* **2019**, *568*, 536−540.
(4) Zhao, X.; Perrin, L.; Procter, D. J.; Maron, L. The Role of H_2O in the Electron Transfer-Activation of Substrates Using SmI_2: Insights from DFT. *Dalton Trans.* **2016**, *45*, 3706−3710.
(5) Ramírez-Solís, A.; Amaro-Estrada, J. I.; Hernández-Cobos, J.; Maron, L. Aqueous Solvation of SmI_2: A Born−Oppenheimer Molecular Dynamics Density Functional Theory Cluster Approach. *J. Phys. Chem. A* **2017**, *121*, 2293−2297.
(6) Huang, H.-M.; McDouall, J. J. W.; Procter, D. J. SmI_2-Catalysed Cyclization Cascades by Radical Relay. *Nat. Catal.* **2019**, *2*, 211−218.
(7) Jaoul, A.; Nocton, G.; Clavaguéra, C. Assessment of Density Functionals for Computing Thermodynamic Properties of Lanthanide Complexes. *ChemPhysChem* **2017**, *18*, 2688−2696.
(8) Kefalidis, C. E.; Perrin, L.; Maron, L. Preliminary Theoretical Insights into SmI_2-Mediated Reactions: Activation of Ketones in THF. *Eur. J. Inorg. Chem.* **2013**, *2013*, 4042−4049.
(9) Castro, L.; Kefalidis, C. E.; McKay, D.; Essafi, S.; Perrin, L.; Maron, L. Theoretical Treatment of One Electron Redox Transformation of a Small Molecule Using F-Element Complexes. *Dalton Trans.* **2014**, *43*, 12124−12134.
(10) Perdew, J. P.; Schmidt, K. Jacob's Ladder of Density Functional Approximations for the Exchange-Correlation Energy. *AIP Conf. Proc.* **2001**, *577*, 1−20.
(11) Frisch, M. J.; Trucks, G. W.; Schlegel, H. B.; Scuseria, G. E.; Robb, M. A.; Cheeseman, J. R.; Scalmani, G.; Barone, V.; Petersson, G. A.; Nakatsuji, H.; et al. *Gaussian*, 2016; Vol. *16*.
(12) Zhao, Y.; Truhlar, D. G. Design of Density Functionals That Are Broadly Accurate for Thermochemistry, Thermochemical Kinetics, and Nonbonded Interactions. *J. Phys. Chem. A* **2005**, *109*, 5656−5667.
(13) Grimme, S.; Antony, J.; Ehrlich, S.; Krieg, H. A Consistent and Accurate Ab Initio Parametrization of Density Functional Dispersion Correction (DFT-D) for the 94 Elements H-Pu. *J. Chem. Phys.* **2010**, *132*, 154104.
(14) Johnson, E. R.; Becke, A. D. A Unified Density-Functional Treatment of Dynamical, Nondynamical, and Dispersion Correlations. II. Thermochemical and Kinetic Benchmarks. *J. Chem. Phys.* **2008**, *128*, 124105.
(15) Grimme, S.; Ehrlich, S.; Goerigk, L. Effect of the Damping Function in Dispersion Corrected Density Functional Theory. *J. Comput. Chem.* **2011**, *32*, 1456−1465.
(16) Yamamoto, A.; Liu, X.; Arashiba, K.; Konomi, A.; Tanaka, H.; Yoshizawa, K.; Nishibayashi, Y.; Yoshida, H. Coordination Structure of Samarium Diiodide in a Tetrahydrofuran−Water Mixture. *Inorg. Chem.* **2023**, *62*, 5348−5356.
(17) Verma, P.; Varga, Z.; Klein, J. E. M. N.; Cramer, C. J.; Que, L.; Truhlar, D. G. Assessment of Electronic Structure Methods for the Determination of the Ground Spin States of Fe(II), Fe(III) and Fe(IV) Complexes. *Phys. Chem. Chem. Phys.* **2017**, *19*, 13049−13069.
(18) Cramer, C. J.; Truhlar, D. G. Density Functional Theory for Transition Metals and Transition Metal Chemistry. *Phys. Chem. Chem. Phys.* **2009**, *11*, 10757−10816.
(19) Goerigk, L.; Hansen, A.; Bauer, C.; Ehrlich, S.; Najibi, A.; Grimme, S. A Look at the Density Functional Theory Zoo with the Advanced GMTKN55 Database for General Main Group Thermochemistry, Kinetics and Noncovalent Interactions. *Phys. Chem. Chem. Phys.* **2017**, *19*, 32184−32215.
(20) Goerigk, L.; Grimme, S. A Thorough Benchmark of Density Functional Methods for General Main Group Thermochemistry, Kinetics, and Noncovalent Interactions. *Phys. Chem. Chem. Phys.* **2011**, *13*, 6670−6688.
(21) Evans, W. J.; Gummersheimer, T. S.; Ziller, J. W. Coordination Chemistry of Samarium Diiodide with Ethers Including the Crystal Structure of Tetrahydrofuran-Solvated Samarium Diiodide, $SmI_2(THF)_5$. *J. Am. Chem. Soc.* **1995**, *117*, 8999−9002.
(22) Marenich, A. V.; Cramer, C. J.; Truhlar, D. G. Universal Solvation Model Based on Solute Electron Density and on a Continuum Model of the Solvent Defined by the Bulk Dielectric Constant and Atomic Surface Tensions. *J. Phys. Chem. B* **2009**, *113*, 6378−6396.
(23) Dunning, T. H. Gaussian Basis Sets for Use in Correlated Molecular Calculations. I. The Atoms Boron through Neon and Hydrogen. *J. Chem. Phys.* **1989**, *90*, 1007−1023.
(24) Kendall, R. A.; Dunning, T. H.; Harrison, R. Electron affinities of the first-row atoms revisited. Systematic basis sets and wave functions. *J. Chem. Phys.* **1992**, *96*, 6796−6806.
(25) Peterson, K. A.; Dunning, T. H. Accurate Correlation Consistent Basis Sets for Molecular Core−Valence Correlation Effects: The Second Row Atoms Al−Ar, and the First Row Atoms B−Ne Revisited. *J. Chem. Phys.* **2002**, *117*, 10548−10560.
(26) Woon, D. E.; Dunning, T. H. Gaussian Basis Sets for Use in Correlated Molecular Calculations. III. The Atoms Aluminum through Argon. *J. Chem. Phys.* **1993**, *98*, 1358−1371.
(27) Woon, D. E.; Dunning, T. H. Gaussian Basis Sets for Use in Correlated Molecular Calculations. V. Core-valence Basis Sets for Boron through Neon. *J. Chem. Phys.* **1995**, *103*, 4572−4585.
(28) Peterson, K. A.; Figgen, D.; Goll, E.; Stoll, H.; Dolg, M. Systematically Convergent Basis Sets with Relativistic Pseudopotentials. II. Small-Core Pseudopotentials and Correlation Consistent Basis Sets for the Post-d Group 16−18 Elements. *J. Chem. Phys.* **2003**, *119*, 11113−11123.
(29) Peterson, K. A.; Shepler, B. C.; Figgen, D.; Stoll, H. On the Spectroscopic and Thermochemical Properties of ClO, BrO, IO, and Their Anions. *J. Phys. Chem. A* **2006**, *110*, 13877−13883.
(30) Dolg, M.; Stoll, H.; Savin, A.; Preuss, H. Energy-Adjusted Pseudopotentials for the Rare Earth Elements. *Theor. Chim. Acta* **1989**, *75*, 173−194.
(31) Dolg, M.; Stoll, H.; Preuss, H. A Combination of Quasirelativistic Pseudopotential and Ligand Field Calculations for Lanthanoid Compounds. *Theor. Chim. Acta* **1993**, *85*, 441−450.
(32) Pritchard, B. P.; Altarawy, D.; Didier, B.; Gibson, T. D.; Windus, T. L. New Basis Set Exchange: An Open, Up-to-Date Resource for the Molecular Sciences Community. *J. Chem. Inf. Model.* **2019**, *59*, 4814−4820.
(33) Feller, D. The Role of Databases in Support of Computational Chemistry Calculations. *J. Comput. Chem.* **1996**, *17*, 1571−1586.
(34) Schuchardt, K. L.; Didier, B. T.; Elsethagen, T.; Sun, L. S.; Gurumoorthi, V.; Chase, J.; Li, J.; Windus, T. L. Basis Set Exchange: A Community Database for Computational Sciences. *J. Chem. Inf. Model.* **2007**, *47*, 1045−1052.
(35) Energy-consistent Pseudopotentials of the Stuttgart/Cologne Group. http://www.tc.uni-koeln.de/PP/clickpse.en.html (accessed Nov 20, 2022).
(36) Glendening, E. D.; Badenhoop, J. K.; Reed, A. E.; Carpenter, J. E.; Bohmann, J. A.; Morales, C. M.; Karafiloglou, P.; Landis, C. R.; Weinhold, F. *NBO 7.0*; Theoretical Chemistry Institute, University of Wisconsin: Madison (WI), 2018.
(37) Cao, X. Y.; Dolg, M. Segmented Contraction Scheme for Small-Core Lanthanide Pseudopotential Basis Sets. *J. Mol. Struct.: THEOCHEM* **2002**, *581*, 139−147.
(38) Dolg, M.; Stoll, H.; Preuss, H. Energy-Adjusted Abinitio Pseudopotentials for the Rare-Earth Elements. *J. Chem. Phys.* **1989**, *90*, 1730−1734.
(39) Neese, F. Software Update: The ORCA Program System—Version 5.0. *Wiley Interdiscip. Rev.: Comput. Mol. Sci.* **2022**, *12*, No. e1606.
(40) Douglas, M.; Kroll, N. M. Quantum Electrodynamical Corrections to the Fine Structure of Helium. *Ann. Phys.* **1974**, *82*, 89−155.
(41) Hess, B. A. Relativistic Electronic-Structure Calculations Employing a Two-Component No-Pair Formalism with External-Field Projection Operators. *Phys. Rev. A* **1986**, *33*, 3742−3748.

https://doi.org/10.1021/acs.jpca.3c00418
J. Phys. Chem. A 2023, 127, 3796−3803

(42) Angeli, C.; Cimiraglia, R.; Malrieu, J.-P. N-Electron Valence State Perturbation Theory: A Fast Implementation of the Strongly Contracted Variant. *Chem. Phys. Lett.* **2001**, *350*, 297−305.
(43) Angeli, C.; Cimiraglia, R.; Evangelisti, S.; Leininger, T.; Malrieu, J.-P. Introduction of N-Electron Valence States for Multireference Perturbation Theory. *J. Chem. Phys.* **2001**, *114*, 10252−10264.
(44) Angeli, C.; Cimiraglia, R.; Malrieu, J.-P. N-Electron Valence State Perturbation Theory: A Spinless Formulation and an Efficient Implementation of the Strongly Contracted and of the Partially Contracted Variants. *J. Chem. Phys.* **2002**, *117*, 9138−9153.
(45) Angeli, C.; Borini, S.; Cestari, M.; Cimiraglia, R. A Quasidegenerate Formulation of the Second Order N-Electron Valence State Perturbation Theory Approach. *J. Chem. Phys.* **2004**, *121*, 4043−4049.
(46) Lang, L.; Sivalingam, K.; Neese, F. The Combination of Multipartitioning of the Hamiltonian with Canonical Van Vleck Perturbation Theory Leads to a Hermitian Variant of Quasidegenerate N-Electron Valence Perturbation Theory. *J. Chem. Phys.* **2020**, *152*, 014109.
(47) Neese, F. Efficient and Accurate Approximations to the Molecular Spin-Orbit Coupling Operator and Their Use in Molecular g-Tensor Calculations. *J. Chem. Phys.* **2005**, *122*, 034107.
(48) Weigend, F.; Ahlrichs, R. Balanced Basis Sets of Split Valence, Triple Zeta Valence and Quadruple Zeta Valence Quality for H to Rn: Design and Assessment of Accuracy. *Phys. Chem. Chem. Phys.* **2005**, *7*, 3297−3305.
(49) Rolfes, J. D.; Neese, F.; Pantazis, D. A. All-Electron Scalar Relativistic Basis Sets for the Elements Rb−Xe. *J. Comput. Chem.* **2020**, *41*, 1842−1849.
(50) Aravena, D.; Neese, F.; Pantazis, D. A. Improved Segmented All-Electron Relativistically Contracted Basis Sets for the Lanthanides. *J. Chem. Theory Comput.* **2016**, *12*, 1148−1156.
(51) Weigend, F. Accurate Coulomb-Fitting Basis Sets for H to Rn. *Phys. Chem. Chem. Phys.* **2006**, *8*, 1057−1065.
(52) Pantazis, D. A.; Neese, F. All-Electron Scalar Relativistic Basis Sets for the Lanthanides. *J. Chem. Theory Comput.* **2009**, *5*, 2229−2238.
(53) Ribeiro, R. F.; Marenich, A. V.; Cramer, C. J.; Truhlar, D. G. Use of Solution-Phase Vibrational Frequencies in Continuum Models for the Free Energy of Solvation. *J. Phys. Chem. B* **2011**, *115*, 14556−14562.
(54) Martin, W. C.; Zalubas, R.; Hagan, L. Atomic Energy Levels - the Rare Earth Elements. (the Spectra of Lanthanum, Cerium, Praseodymium, Neodymium, Promethium, Samarium, Europium, Gadolinium, Terbium, Dysprosium, Holmium, Erbium, Thulium, Ytterbium, and Lutetium). [66 Atoms and Ions]; PB-282067; NSRDS-NBS-60; Manchester Coll. of Science and Technology (UK), Dept. of Chemistry, 1978; pp 181−183. https://www.osti.gov/biblio/6507735 (retrieved March 20, 2023).
(55) Mortensen, S. S.; Marciniak Nielsen, M. A.; Nawrocki, P.; Sørensen, T. J. Electronic Energy Levels and Optical Transitions in Samarium(III) Solvates. *J. Phys. Chem. A* **2022**, *126*, 8596−8605.
(56) Carnall, W. T.; Fields, P. R.; Rajnak, K. Electronic Energy Levels in the Trivalent Lanthanide Aquo Ions. I. Pr^{3+}, Nd^{3+}, Pm^{3+}, Sm^{3+}, Dy^{3+}, Ho^{3+}, Er^{3+}, and Tm^{3+}. *J. Chem. Phys.* **1968**, *49*, 4424−4442.
(57) Enemærke, R. J.; Daasbjerg, K.; Skrydstrup, T. Is Samarium Diiodide an Inner- or Outer-Sphere Electron Donating Agent? *Chem. Commun.* **1999**, 343−344.
(58) Mai, C.-L.; Moehl, T.; Hsieh, C.-H.; Décoppet, J.-D.; Zakeeruddin, S. M.; Grätzel, M.; Yeh, C.-Y. Porphyrin Sensitizers Bearing a Pyridine-Type Anchoring Group for Dye-Sensitized Solar Cells. *ACS Appl. Mater. Interfaces* **2015**, *7*, 14975−14982.
(59) Pan, B.; Zhu, Y.-Z.; Ye, D.; Zheng, J.-Y. Improved Conversion Efficiency in Dye-Sensitized Solar Cells Based on Porphyrin Dyes with Dithieno[3,2-b:2′,3′-d]Pyrrole Donor. *Dyes Pigm.* **2018**, *150*, 223−230.
(60) Trasatti, S. The Absolute Electrode Potential: An Explanatory Note (Recommendations 1986). *Pure Appl. Chem.* **1986**, *58*, 955−966.
(61) Isse, A. A.; Gennaro, A. Absolute Potential of the Standard Hydrogen Electrode and the Problem of Interconversion of Potentials in Different Solvents. *J. Phys. Chem. B* **2010**, *114*, 7894−7899.
(62) Bryenton, K. R.; Adeleke, A. A.; Dale, S. G.; Johnson, E. R. Delocalization Error: The Greatest Outstanding Challenge in Density-Functional Theory. *Wiley Interdiscip. Rev.: Comput. Mol. Sci.* **2023**, *13*, No. e1631.
(63) Santra, G.; Sylvetsky, N.; Martin, J. M. L. Minimally Empirical Double-Hybrid Functionals Trained against the GMTKN55 Database: RevDSD-PBEP86-D4, RevDOD-PBE-D4, and DOD-SCAN-D4. *J. Phys. Chem. A* **2019**, *123*, 5129−5143.
(64) Duignan, T. J.; Autschbach, J. Impact of the Kohn−Sham Delocalization Error on the 4f Shell Localization and Population in Lanthanide Complexes. *J. Chem. Theory Comput.* **2016**, *12*, 3109−3121.
(65) Warren, J. J.; Tronic, T. A.; Mayer, J. M. Thermochemistry of Proton-Coupled Electron Transfer Reagents and its Implications. *Chem. Rev.* **2010**, *110*, 6961−7001.
(66) Tanabe, Y.; Nishibayashi, Y. Comprehensive Insights into Synthetic Nitrogen Fixation Assisted by Molecular Catalysts under Ambient or Mild Conditions. *Chem. Soc. Rev.* **2021**, *50*, 5201−5242.
(67) Kolmar, S. S.; Mayer, J. M. $SmI_2(H_2O)_n$ Reduction of Electron Rich Enamines by Proton-Coupled Electron Transfer. *J. Am. Chem. Soc.* **2017**, *139*, 10687−10692.
(68) Szostak, M.; Spain, M.; Procter, D. J. Determination of the Effective Redox Potentials of SmI_2, $SmBr_2$, $SmCl_2$, and Their Complexes with Water by Reduction of Aromatic Hydrocarbons. Reduction of Anthracene and Stilbene by Samarium(II) Iodide−Water Complex. *J. Org. Chem.* **2014**, *79*, 2522−2537.
(69) Gagné, O. C. Bond-Length Distributions for Ions Bonded to Oxygen: Results for the Lanthanides and Actinides and Discussion of the f-Block Contraction. *Acta Crystallogr., Sect. B: Struct. Sci., Cryst. Eng. Mater.* **2018**, *74*, 49−62.
(70) Grimme, S. Semiempirical Hybrid Density Functional with Perturbative Second-Order Correlation. *J. Chem. Phys.* **2006**, *124*, 034108.
(71) Kozuch, S.; Martin, J. M. L. DSD-PBEP86: In Search of the Best Double-Hybrid DFT with Spin-Component Scaled MP2 and Dispersion Corrections. *Phys. Chem. Chem. Phys.* **2011**, *13*, 20104−20107.
(72) Brémond, É.; Sancho-García, J. C.; Pérez-Jiménez, Á. J.; Adamo, C. Communication: Double-Hybrid Functionals from Adiabatic-Connection: The QIDH Model. *J. Chem. Phys.* **2014**, *141*, 031101.
(73) Sancho-García, J. C.; Brémond, É.; Savarese, M.; Pérez-Jiménez, A. J.; Adamo, C. Partnering Dispersion Corrections with Modern Parameter-Free Double-Hybrid Density Functionals. *Phys. Chem. Chem. Phys.* **2017**, *19*, 13481−13487.
(74) Martin, J. M. L.; Santra, G. Empirical Double-Hybrid Density Functional Theory: A 'Third Way' in Between WFT and DFT. *Isr. J. Chem.* **2020**, *60*, 787−804.
(75) Brémond, E.; Ciofini, I.; Sancho-García, J. C.; Adamo, C. Nonempirical Double-Hybrid Functionals: An Effective Tool for Chemists. *Acc. Chem. Res.* **2016**, *49*, 1503−1513.
(76) Chai, J.-D.; Head-Gordon, M. Long-Range Corrected Hybrid Density Functionals with Damped Atom−Atom Dispersion Corrections. *Phys. Chem. Chem. Phys.* **2008**, *10*, 6615−6620.
(77) Purvis, G. D.; Bartlett, R. J. A Full Coupled-cluster Singles and Doubles Model: The Inclusion of Disconnected Triples. *J. Chem. Phys.* **1982**, *76*, 1910−1918.
(78) Lee, T. J.; Taylor, P. R. A Diagnostic for Determining the Quality of Single-Reference Electron Correlation Methods. *Int. J. Quantum Chem.* **2009**, *36*, 199−207.

https://doi.org/10.1021/acs.jpca.3c00418
J. Phys. Chem. A 2023, 127, 3796−3803